

## Loss of autophagy in chondrocytes causes severe growth retardation

Yoji Horigome<sup>a,b,#</sup>, Hiroko Ida-Yonemochi<sup>c,#</sup>, Satoshi Waguri<sup>d</sup>, Shunichi Shibata<sup>e</sup>, Naoto Endo<sup>b</sup>, and Masaaki Komatsu<sup>a,f</sup>

<sup>a</sup>Department of Biochemistry, Niigata University Graduate School of Medical and Dental Sciences, Chuo-ku, Japan; <sup>b</sup>Division of Orthopedic Surgery Department of Regeneration and Transplant Medicine, Niigata University Graduate School of Medical and Dental Sciences, Chuo-ku, Japan; <sup>c</sup>Division of Anatomy and Cell Biology of the Hard Tissue, Department of Tissue Regeneration and Reconstruction, Niigata University Graduate School of Medical and Dental Sciences, Chuo-ku, Japan; <sup>d</sup>Department of Anatomy and Histology, Fukushima Medical University School of Medicine, Hikarigaoka, Japan; <sup>e</sup>Department of Maxillofacial Anatomy, Graduate School of Medical and Dental Sciences, Tokyo Medical and Dental University, Tokyo, Japan; <sup>f</sup>Department of Physiology, Juntendo University Graduate School of Medicine, Tokyo, Japan

### ABSTRACT

Chondrogenesis is accompanied by not only cellular renovation, but also metabolic stress. Therefore, macroautophagy/autophagy is postulated to be involved in this process. Previous reports have shown that suppression of autophagy during chondrogenesis causes mild growth retardation. However, the role of autophagy in chondrocyte differentiation still largely remains unclear. Here, we show the important role of autophagy on chondrogenesis. The transition of mesenchymal cells to chondrocytes was severely impaired by ablation of *Atg7*, a gene essential for autophagy. Mice lacking *Atg7* after the transition exhibited phenotypes severer than mutant mice in which *Atg7* was removed before the transition. *Atg7*-deficient chondrocytes accumulated large numbers of glycogen granules, hardly proliferate and died specifically in the proliferative zone without any ER-stress signal. Our results suggest that the suppression of autophagy in prechondrogenic cells drives compensatory mechanism(s) that mitigate defective chondrogenesis, and that autophagy participates in glycogenolysis to supply glucose in avascular growth plates.

**Abbreviations:** DDIT3/CHOP: DNA damage inducible transcript 3; ER: endoplasmic reticulum; NFE2L2/NRF2: nuclear factor, erythroid derived 2, like 2; SQSTM1/p62: sequestosome 1; STBD1: starch-binding domain-containing protein 1

### ARTICLE HISTORY

Received 24 January 2019  
Revised 18 May 2019  
Accepted 28 May 2019

### KEYWORDS

*Atg7*; autophagy; cartilage; chondrogenesis; glycogenolysis

## Introduction


Autophagy is an intracellular degradation pathway that takes place in lysosomes. Macroautophagy (hereafter referred to as autophagy), the best-characterized form of autophagy, is accompanied by formation of an autophagosome, which surrounds a portion of cytoplasm and eventually fuses with the lysosome, which contains various hydrolases, including proteases, lipases, glycosidases, and nucleases [1]. This degradation system is induced by a variety of stresses, including nutrient deprivation, and enables the cell to adapt to environmental conditions. Therefore, autophagy provides molecular building blocks, such as amino acids, glucose, nucleotides, and fatty acids, for use by cells under stress conditions, and it also removes unnecessary, excessive, or damaged macromolecules, including organelles [2,3]. Mouse models of defective autophagy have shown that autophagy is required to maintain the levels of amino acids and glucose in blood and tissues of neonatal and adult mice during fasting [4,5]. Autophagic degradation of lipid droplets in lysosomes is thought to contribute to mobilization of triglycerides during starvation [6]. Supply of lipids through autophagy is also required to

replenish triglycerides in lipid droplets [7]. During the neonatal starvation period, expression of the gene encoding lysosomal acid GAA (glucosidase, alpha, acid) is induced in the liver, and glycogen granules are degraded by autophagy for catabolism into glucose [8,9]. Autophagy is also needed for cellular differentiation and regeneration, both of which are accompanied by bulk replacement of the cytoplasmic components, including organelles [10]. Experiments with genetically modified mice revealed indispensable roles of autophagy in adipogenesis [6,11], erythroid differentiation [12], early embryogenesis [13], hepatic regeneration [14], and the beige-to-white adipocyte transition [15].

Chondrogenesis is a dynamic process that is accompanied by not only changes in cell properties and morphology, but also metabolic stress [16]. During endochondral bone development, mesenchymal cells undergo condensation, which is followed by differentiation of prechondrogenic cells within these condensations into round chondrocytes. Round chondrocytes in cartilage proliferate and progressively reach a stage in which they produce substantial collagen fibrils and proteoglycans and secrete them into extracellular space. Proliferating chondrocytes in the central region of the cartilage then exit

**CONTACT** Masaaki Komatsu  [mkomatsu@juntendo.ac.jp](mailto:mkomatsu@juntendo.ac.jp)  Department of Biochemistry, Niigata University Graduate School of Medical and Dental Sciences, Chuo-ku 951-8510, Japan

<sup>#</sup>These two authors contributed equally to this work.

 The supplementary data for this article can be accessed here.

© 2019 The Author(s). Published by Informa UK Limited, trading as Taylor & Francis Group.

This is an Open Access article distributed under the terms of the Creative Commons Attribution-NonCommercial-NoDerivatives License (<http://creativecommons.org/licenses/by-nc-nd/4.0/>), which permits non-commercial re-use, distribution, and reproduction in any medium, provided the original work is properly cited, and is not altered, transformed, or built upon in any way.

the cell cycle and differentiate into hypertrophic chondrocytes. The proliferating chondrocytes closest to the hypertrophic chondrocytes flatten out and form orderly columns of flat chondrocytes, which continue to proliferate. Eventually, hypertrophic chondrocytes die, and their cartilage lacuna are invaded by blood vessels along with osteoblasts and osteoclasts, which then replace the cartilage with newly formed bone matrix. Because the epiphyseal growth plate is an avascular structure, nutrients and oxygen diffuse from the metaphyseal side of the growth plate, suggesting that chondrocytes in the middle of the growth plate experience malnutrition and hypoxia [17,18].

Autophagy is postulated to be involved in chondrogenesis, in terms of both the nutrient supply and the replacement of cellular components, as well as tolerance of endoplasmic reticulum (ER) stress. In fact, during chondrogenesis in the early postnatal stage, autophagy is induced throughout the growth plate, a process mediated by FGF18 through FGFR4 and JNK-dependent activation of the autophagy initiation complex PIK3C3/VPS34-BECN1/Beclin 1 [19]. Ablation of the autophagy-related gene *Atg5* or *Atg7* during chondrogenesis causes mild growth retardation accompanied by enhanced chondrocyte cell death and reduced cell proliferation [20,21]. ER-stress mediated cell death occurs in growth plate chondrocytes lacking *Atg7*, which leads to mild growth retardation [21]. Targeted deletion of *Atg5* in chondrocytes promotes age-related osteoarthritis [22]. These findings were based on data utilizing *Col2a1-* and *Prdx1/Prx1-Cre* transgenic mice that express Cre recombinase at the stage of mesenchymal condensation and in mesenchymal cells, respectively [23–25]. In this study, using *Col11a2/11Enh-Cre* transgenic mice that express Cre recombinase at the round proliferative chondrocyte stage [26], we found that suppression of autophagy during chondrogenesis causes increased apoptosis and reduced growth of proliferative chondrocytes in the absence of ER stress, leading to severe growth retardation.

## Results

### Indispensable role of autophagy in the transition of mesenchymal cells to proliferative chondrocytes

ATDC5 cells grown *in vitro* recapitulate multistep differentiation process encompassing the stages from mesenchymal condensation to calcification [27]. To investigate the role of autophagy in chondrogenesis, we generated *Atg7*-deficient ATDC5 cells (Figure S1(a)). Loss of *Atg7* in ATDC5 cells inhibited the conversion of LC3-I to LC3-II [28] and led to the accumulation of autophagy-specific substrate, SQSTM1/p62 [29] (Figure S1(a)), indicating suppression of autophagy. Treatment of ATDC5 cells with INSULIN leads to chondrogenic differentiation that involves formation of cartilage nodules through a cellular condensation process, which gives rise to proliferating chondrocytes. The cartilage nodules increase in size due to chondrocyte proliferation, which continues for about 14 d and then ceases by 21 d [27]. In wild-type ATDC5 cells, COL2A1/COLLAGEN II, which is mainly expressed in proliferative chondrocytes, was detectable 16 d after INSULIN treatment, and the level increased over time

(Figure S1(b)). In marked contrast, expression of COL2A1 in *Atg7*-deficient ATDC5 cells was almost completely blocked (Figure S1(b)). These results suggested that autophagy is needed for the transition of mesenchymal cells into proliferating chondrocytes.

### Generation of *atg7<sup>fllox/fllox</sup>*; *Col11a2-Cre* mice

In previous studies, *Col2a1-* or *Prdx1-Cre* transgenic mice that express Cre recombinase prior to chondrocyte differentiation were utilized to investigate the role of autophagy in cartilage [19–22]. However, as shown in Figure S1, autophagy seems to be involved in the differentiation of mesenchymal cells into round chondrocytes, raising the possibility that autophagy-deficient models using *Col2a1-* and *Prdx1-Cre* transgenic mice have a defect in an early differentiation step, potentially masking the role of autophagy in chondrocytes. To exclude the effect of defective autophagy in mesenchymal and prechondrogenic cells on chondrogenesis, we crossbred *Atg7<sup>fllox/fllox</sup>* mice [30] with *Col11a2-Cre* transgenic mice that express Cre recombinase at the step of round proliferative chondrocytes [26]. The amount of ATG7 protein in cartilage of *atg7<sup>fllox/fllox</sup>*; *Col11a2-Cre* mice was significantly lower than in cartilage of control mice (Figure 1(a)). Conversion of LC3-I to LC3-II was markedly impaired, and SQSTM1 accumulated in mutant cartilage though not statistically significant (Figure 1(a)). Double immunofluorescence analysis with anti-ATG7 and anti-SQSTM1 antibodies revealed loss of signal for ATG7 protein and accumulation of SQSTM1-positive structures, a hallmark of defective autophagy, in resting to hypertrophic chondrocytes of *atg7<sup>fllox/fllox</sup>*; *Col11a2-Cre* mice, but not in age-matched control mice (Figure 1(b)). Immunofluorescence analysis with anti-LC3 antibody revealed LC3 puncta in both proliferative and hypertrophic chondrocytes of *Atg7<sup>fllox/fllox</sup>* mice but not in of *atg7<sup>fllox/fllox</sup>*; *Col11a2-Cre* mice (Figure 1(c)). These results indicated suppression of autophagy starting at the resting chondrocyte stage in *atg7<sup>fllox/fllox</sup>*; *Col11a2-Cre* mice.

### *Atg7<sup>fllox/fllox</sup>*; *Col11a2-Cre* mice show severe growth retardation

*atg7<sup>fllox/fllox</sup>*; *Col11a2-Cre* mice were born at the predicted Mendelian ratio, and were fertile; however, the mutant mice exhibited severe growth retardation. Body weight and length were both lower in mutant mice at 3 and 6 weeks of age than in age-matched control mice (3 weeks body weight: 28.3%,  $n = 5$ ,  $p < 0.01$ ; 6 weeks body weight: 14.5%,  $n = 7$ ,  $p < 0.01$ ; 3 weeks body length: 11.5%,  $n = 5$ ,  $p < 0.01$ ; 6 weeks body length: 7.9%,  $n = 5$ ,  $p < 0.01$ ) (Figure 2(a–b)). Both X-ray examination and staining with Alcian blue and alizarin red S revealed a significant decrease in the bone length of mutant mice at 3 and 6 weeks of age relative to age-matched controls (Figure 2(c–d)). Long bones (humerus, ulna, femur, and tibia) of mutant mice were shorter than that of control mice at both 3 and 6 weeks of age (3 weeks: 17.1, 21.2, 20.7 and 18.7%,  $n = 3$ , respectively,  $p < 0.01$ ; 6 weeks: 20.6, 14.6, 21.9 and 17.5%,  $n = 6$ , respectively,  $p < 0.01$ ) (Figure 2(e)). These phenotypes were more severe in *atg7<sup>fllox/fllox</sup>*; *Col11a2-Cre* mice than in *atg7<sup>fllox/fllox</sup>*; *Col2a1-Cre*, *atg7<sup>fllox/fllox</sup>*; *Tam<sup>Col2a1-Cre</sup>* and *atg7<sup>fllox/fllox</sup>*; *Prdx1-Cre* (Table 1) [19–21].

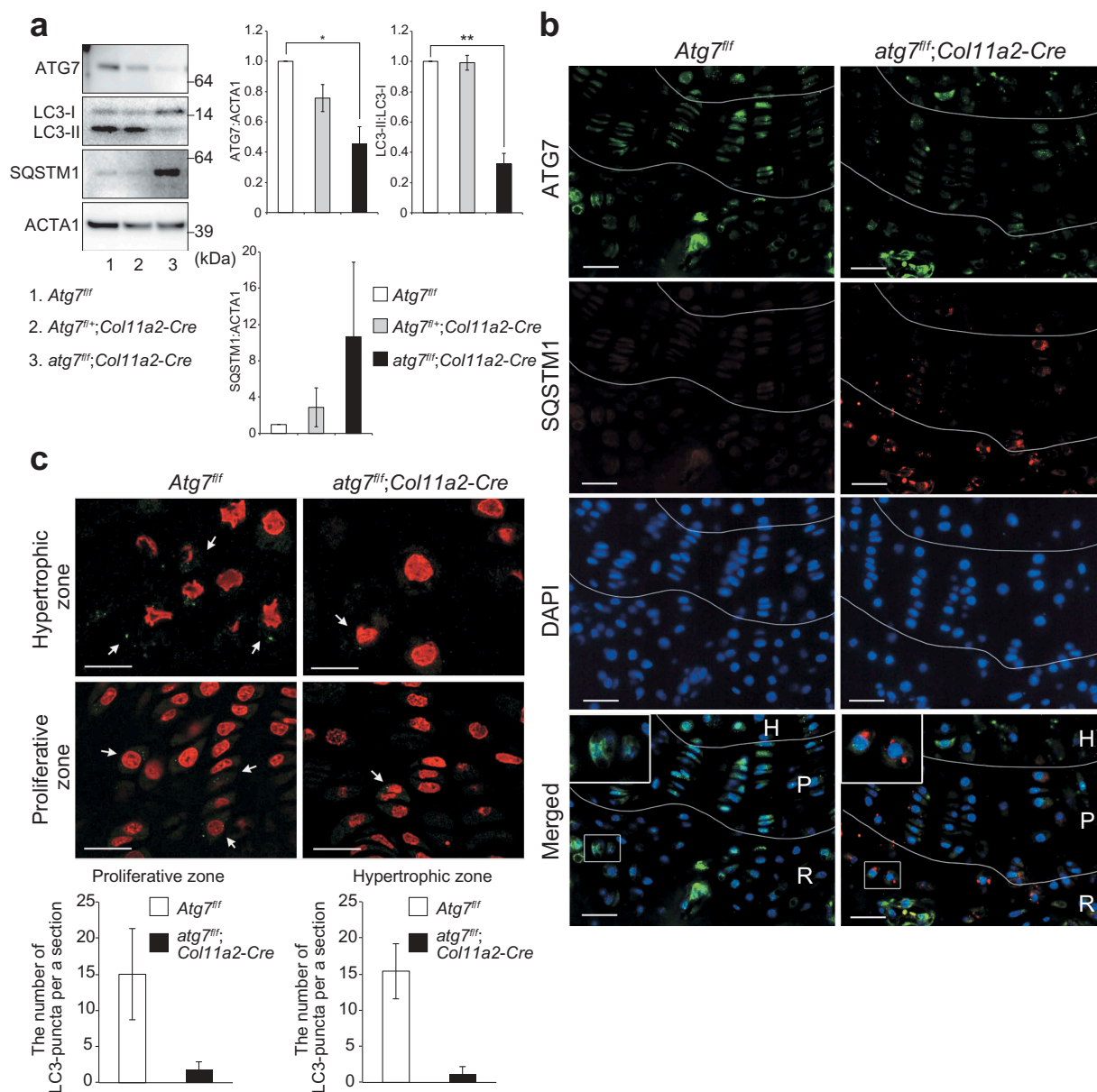


**Figure 1.** Impairment of autophagy in chondrocytes of *atg7<sup>fllox/fllox</sup>, Col11a2-Cre* mice. **(a)** Immunoblot analysis. Lysates prepared from femur cartilages of mice of the indicated genotype at postnatal day 3 were subjected to immunoblotting with anti-ATG7, anti-LC3, anti-SQSTM1, and anti-ACTA1 antibodies. Data are representative of 3 separate experiments. Bar graphs indicate the quantitative densitometric analyses of ATG7 relative to ACTA1, LC3-II relative to LC3-I, and SQSTM1 relative to ACTA1. Data are means  $\pm$  s.e.m. \* $P < 0.05$  and \*\* $P < 0.01$ , as determined by Welch's *t*-test. **(b)** Immunohistochemistry microscopy. Femur cartilage sections of *Atg7<sup>fllox/fllox</sup>* and *atg7<sup>fllox/fllox</sup>, Col11a2-Cre* mice aged 6 weeks were immunostained with anti-ATG7 and anti-SQSTM1 antibodies. Bars: 50  $\mu$ m. R: resting zone, P: proliferative zone, H: hypertrophic zone. **(c)** Immunohistochemistry microscopy. Femur cartilage sections of *Atg7<sup>fllox/fllox</sup>* and *atg7<sup>fllox/fllox</sup>, Col11a2-Cre* mice aged 3 weeks were immunostained with anti-LC3 antibody. Arrows indicate chondrocytes harboring LC3-positive puncta. Bars: 20  $\mu$ m. Graphs represent the average number of LC3-positive puncta in a section of hypertrophic (upper) and proliferative zones (bottom) of the indicated genotypes ( $n = 5$ ).

Hematoxylin-Eosin staining exhibited a disorganized growth plate in *atg7<sup>fllox/fllox</sup>, Col11a2-Cre* at 3 weeks and 6 weeks of age (Figure 3(a) and data not shown). Although there was no significant difference in the thickness of the growth plate among genotypes (Figure 3(b)), we observed obvious swelling of both proliferating and hypertrophic chondrocytes in the femurs of *atg7<sup>fllox/fllox</sup>, Col11a2-Cre* (Figure 3(c)). Although TUNEL staining revealed marked cell death of mutant chondrocytes specifically in the proliferating zone (Figure 3(d)), immunohistochemical staining with anti-MKI67 antibody revealed reduced growth of proliferative chondrocytes (Figure 3(e)). These results suggest that suppression of autophagy starting at the resting chondrocyte stage

affects survival and proliferation of chondrocytes in the proliferative zone.

#### Slight er-stress signaling in autophagy-deficient chondrocytes

In the next series of experiments, we investigated whether loss of autophagy in chondrocytes affects production and secretion of collagen fibrils such as COL2A1 and COL10A1/type X COLLAGENS. Immunohistochemical analysis with anti-COL2A1 and -COL10A1 antibodies revealed high levels

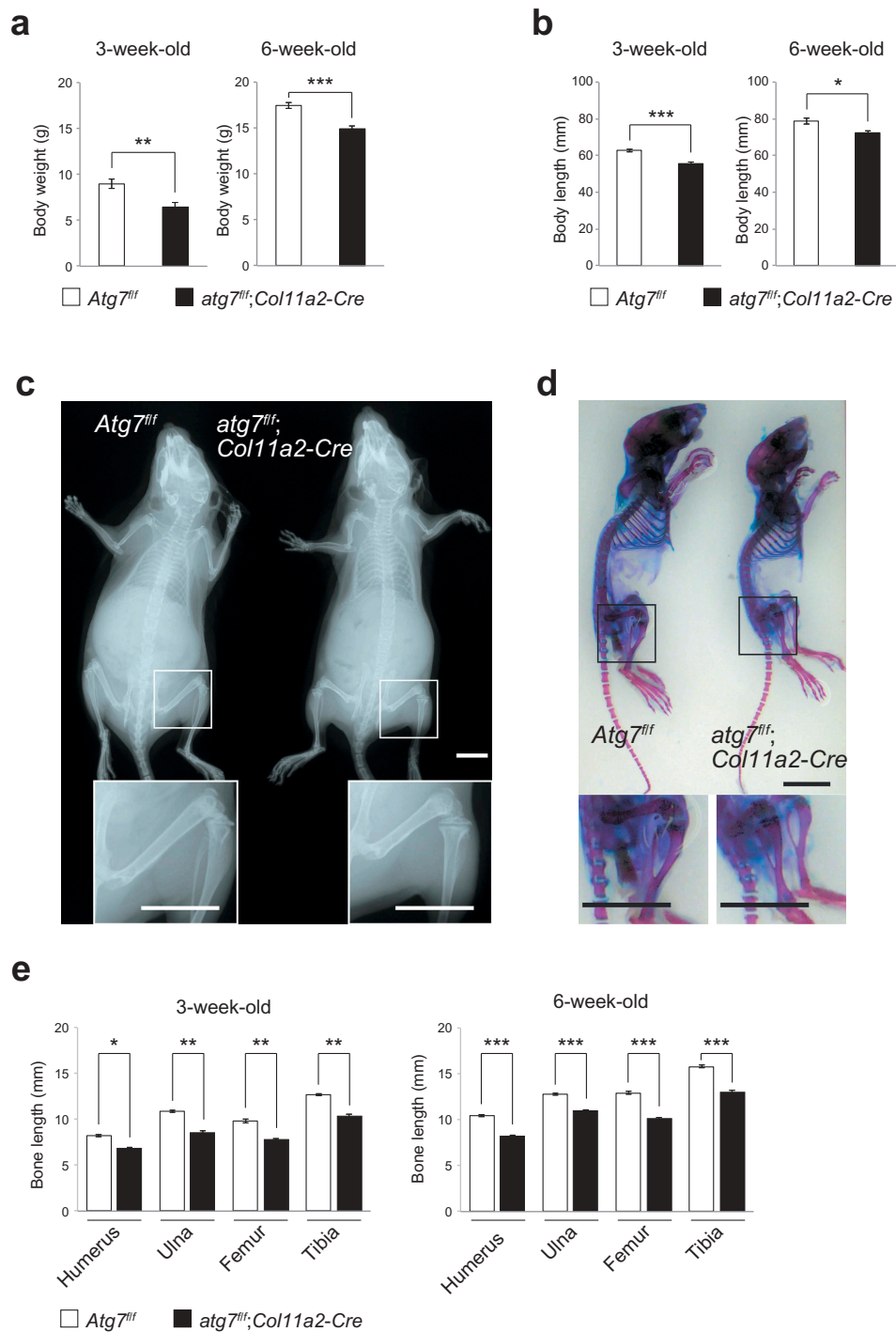


**Figure 2.** *atg7<sup>fllox/fllox</sup>; Col11a2-Cre* mice exhibit growth retardation. **(a)** Body weight of *Atg7<sup>fllox/fllox</sup>* and *atg7<sup>fllox/fllox</sup>; Col11a2-Cre* mice aged 3 (n = 5) and 6 weeks (n = 6). Data are means  $\pm$  s.e.m.  $**P < 0.01$  and  $***P < 0.001$ , as determined by Welch's *t*-test. **(b)** Body length of *Atg7<sup>fllox/fllox</sup>* and *atg7<sup>fllox/fllox</sup>; Col11a2-Cre* mice aged 3 (n = 3) and 6 weeks (n = 7). Data are means  $\pm$  s.e.m.  $*P < 0.05$  and  $***P < 0.001$ , as determined by Welch's *t*-test. **(c)** Representative X-ray image of *Atg7<sup>fllox/fllox</sup>* and *atg7<sup>fllox/fllox</sup>; Col11a2-Cre* mice aged 6 weeks. Bars: 1 mm. **(d)** Skeletal specimen of *Atg7<sup>fllox/fllox</sup>* and *atg7<sup>fllox/fllox</sup>; Col11a2-Cre* mice aged 3 weeks. Bars: 1 mm. **(e)** Humerus, ulna, femur, and tibia lengths of *Atg7<sup>fllox/fllox</sup>* and *atg7<sup>fllox/fllox</sup>; Col11a2-Cre* mice aged 3 (n = 3) and 6 weeks (n = 6). Data are means  $\pm$  s.e.m.  $*P < 0.05$ ,  $**P < 0.01$ , and  $***P < 0.001$ , as determined by Welch's *t*-test.

of COL2A1 in both chondrocytes and extracellular spaces throughout the resting, proliferative, and hypertrophic zones, regardless of genotype (Figure 4(a)). Both COL2A1 and COL10A1 accumulated moderately in swollen proliferative chondrocytes in the growth plates of 3-week-old *atg7<sup>fllox/fllox</sup>; Col11a2-Cre* mice (Figure 4(a–b)), implying retention

of both COLLAGENS in ER of mutant chondrocytes. The signal intensities increased with age (Figure S2). Indeed, electron microscopic analysis revealed dilated rough ER in chondrocytes from mice of all genotypes (Figure 4(c)), and the number of such structures was significantly higher in mutant chondrocytes than in control chondrocytes (Figure 4



**Table 1.** Phenotypes of different types of cartilage-specific *atg7*-knockout mice.

Genotype/Age	9 d	3 w	4 w	6 w	8 w	120 d	Ref.
<i>atg7<sup>flox/flox</sup>; Col11a2-Cre</i>	-	Femur 20.7%** Tibia 18.7%** Humerus 17.1%* Ulna 21.2%**	-	Femur 21.9%*** Tibia 17.5%*** Humerus 20.6%*** Ulna 14.6%***	-	-	This study
<i>atg7<sup>flox/flox</sup>; Prdx1-Cre</i>	Femur 10%* Tibia 10%*	-	Femur 10%** Tibia 7%*	-	-	Femur 20%** Tibia 15%**	[19]
<i>atg7<sup>flox/flox</sup>; Col2a1-Cre</i>	-	-	Femur 10%* Tibia 5%*	-	Femur 5.1%** Tibia 3.3%**	Femur 15%** Tibia 7%*	[20]
<i>atg7<sup>flox/flox</sup>; Tam<sup>Col2a1-Cre</sup></i>	-	-	Femur 7.8%* Tibia 7.3%*	-	Femur 17.9% Tibia 10.2%	-	[21]

Percentages show reductions in bone length of mice of each genotype at the indicated ages, compared with the corresponding age-matched control mice. \* $P < 0.05$ , \*\* $P < 0.01$ , and \*\*\* $P < 0.001$ .

(c). On the basis of our observation and previous reports [19,21], we speculated that the mutant chondrocytes were undergoing robust ER stress. Surprisingly, however, we did not observe any chondrocytes positive for the ER-stress markers DDIT3/CHOP and HSPA3/BIP in the resting, proliferative, and hypertrophic zones of mutant growth plates (Figure 4(d–e)). Consistent with those histological analyses, immunoblot analysis revealed that DDIT3 was not detectable in the growth plates of *atg7<sup>flox/flox</sup>; Col11a2-Cre* mice at postnatal day 3 or at 3 weeks of age (Figure 4(f)). Considering that cell death of chondrocytes was detectable even in 3-week-old *atg7<sup>flox/flox</sup>; Col11a2-Cre* mice (Figure 3(d)), these results suggest that the ER stress does not make an important contribution to the apoptosis of autophagy-defective proliferative chondrocytes.

### Accumulation of glycogen granules in autophagy-deficient chondrocytes

A unique feature of suppression of autophagy is the accumulation of SQSTM1 and subsequent activation of the transcription factor NFE2L2/NRF2 (nuclear factor, erythroid derived 2, like 2) [31,32]. Because NFE2L2 negatively regulates chondrogenesis [33], we next investigated whether SQSTM1-mediated NFE2L2 activation affects chondrogenesis. To do this, we crossbred *atg7<sup>flox/flox</sup>; Col11a2-Cre* mice with *Sqstm1<sup>flox/flox</sup>* mice [31] to generate chondrocyte-specific *atg7*- and *sqstm1*-double-knockout mice. We verified the disappearance of both ATG7 and SQSTM1 in the cartilages of *atg7<sup>flox/flox</sup>; sqstm1<sup>flox/flox</sup>; Col11a2-Cre* mice (Fig. S3A). Unexpectedly, however, neither growth retardation nor short bone length of *atg7<sup>flox/flox</sup>; Col11a2-Cre* mice were rescued by additional loss of *Sqstm1* (Figure S3(b–d)). Similarly, specific ablation of *Nfe2l2* in chondrocytes neither accelerated chondrogenesis in *atg7<sup>flox/flox</sup>; Col11a2-Cre* mice nor rescued growth retardation or short bone length (data not shown). Taken together, these findings indicated that the accumulation of SQSTM1 barely affected chondrogenesis in *atg7<sup>flox/flox</sup>; Col11a2-Cre* mice.

During chondrogenesis, chondrocytes in the middle of the growth plate suffer from nutrient deprivation due to the avascular structure of growth plate [17,18]. Chondrocytes induce glycogenolysis to provide glucose for energy production and to overcome malnutrition [34,35]. In addition to cytoplasmic glycogenolysis, autophagy also has the ability to

catabolize glycogen granules [1,36]. Thus, we carried out immunohistochemical analysis with anti-glycogen antibody. As shown in Figure 5(a), we observed glycogen in resting and hypertrophic chondrocytes of both control and mutant mice, but the signal intensity was much higher in mutant chondrocytes. This accumulation was observed in chondrocytes as early as 3 weeks in *atg7<sup>flox/flox</sup>; Col11a2-Cre* mice (Figure 5(a)). Consistent with these results, electron microscopy showed that the ratio of glycogen area in mutant chondrocytes was significantly higher than that in control chondrocytes (Figure 5(b)).

### Discussion

In this study, we demonstrated the role of autophagy during chondrogenesis. We found that 1) the transition of mesenchymal cells to chondrocytes is inhibited by suppression of autophagy; 2) loss of autophagy in chondrocytes after the transition causes severe growth retardation and short bone length; 3) autophagy-deficient chondrocytes die in the specifically proliferative zone, which is not involved in ER stress; and 4) autophagy-deficient chondrocytes accumulate massive glycogen granules.

Remarkably, the phenotypes were more severe in *atg7<sup>flox/flox</sup>; Col11a2-Cre* mice than in other chondrocyte-specific autophagy-knockout mice, i.e., the *atg7<sup>flox/flox</sup>; Col2a1-Cre* and *atg7<sup>flox/flox</sup>; Prdx1-Cre* transgenic mice, both of which lack *Atg7* at an earlier step of differentiation than *Col11a2-Cre* transgenic mice (Table 1) [19–21]. Indeed, Vuppapapati *et al.* reported that no significant difference in body and bone length was observed in 1 month-old *atg7<sup>flox/flox</sup>; Col2a1-Cre* mice, and that both *atg7<sup>flox/flox</sup>; Col2a1-Cre* and *atg7<sup>flox/flox</sup>; Col2a1-Cre* mice exhibit mild growth retardation at 2 months of age (femur length: 5.1% decrease, and tibia length: 3.3% decrease) [20], a milder phenotype that we observed in *atg7<sup>flox/flox</sup>; Col11a2-Cre* mice (Figure 2(e)). Mice harboring postnatal deletion of *Atg7* in chondrocytes (*atg7<sup>flox/flox</sup>; Tam<sup>Col2a1-Cre</sup>* mice) experience growth retardation starting at 4 weeks of age [21], but this phenotype is also milder than that of *atg7<sup>flox/flox</sup>; Col11a2-Cre* mice. Long bone (femur and tibia) lengths of *atg7<sup>flox/flox</sup>; Tam<sup>Col2a1-Cre</sup>* mice were 7.8% and 7.3% lower, respectively, than those of controls at 4 weeks of age, and 17.9% and 10.2% lower, respectively, at 8 weeks of age. Even in *atg7<sup>flox/flox</sup>; Prdx1-Cre* mice at postnatal day 30 [19], the lengths of femur and tibia decreased just 10% relative to those of control mice, again a milder phenotype than in *atg7<sup>flox/flox</sup>*;

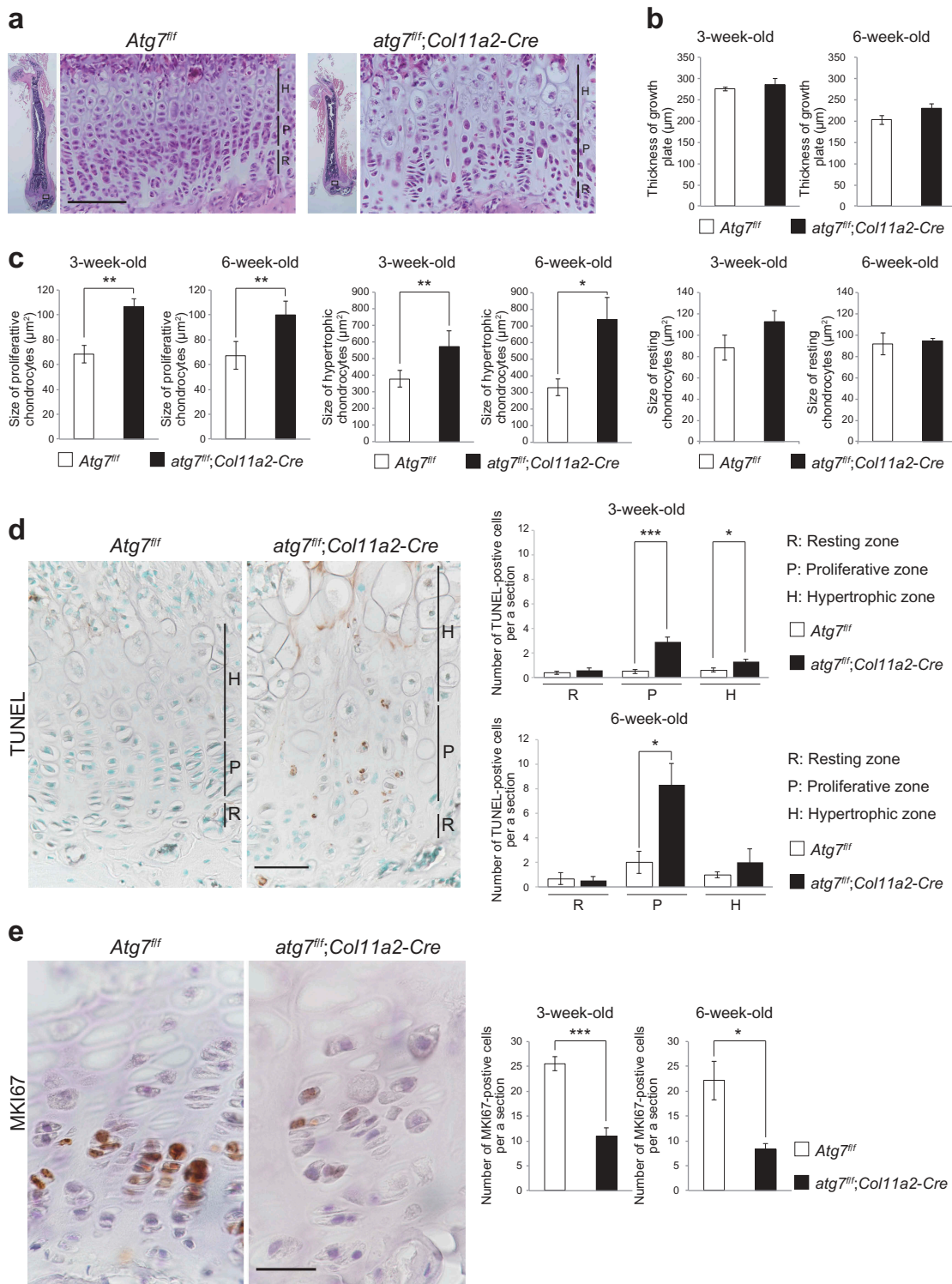


**Figure 3.** Disorganized growth plate of femur of *Atg7<sup>flox/flox</sup>* and *atg7<sup>flox/flox</sup>; Col11a2-Cre* mice. (a) Hematoxylin-Eosin staining of femur of mice of the indicated genotypes at 6 weeks of age. Bars: 1 mm. Each inset is a magnified image. Bar: 100 μm. R: resting zone, P: proliferative zone, H: hypertrophic zone. (b) Thickness of the growth plate among genotypes at 3 (n = 5) and 6 weeks of age (n = 3). Data are means ± s.e.m. \**P* < 0.05 and \*\**P* < 0.01, as determined by Welch's *t*-test. (c) Sizes of proliferative, hypertrophic, and resting chondrocytes among the genotypes described in (b). Data are means ± s.e.m. \**P* < 0.05 and \*\*\**P* < 0.001, as determined by Welch's *t*-test. (d) TUNEL staining of femur described in (b). R: resting zone, P: proliferative zone, H: hypertrophic zone. Bars: 50 μm. Graphs represent the number of TUNEL-positive cells in a section of growth plate of indicated genotypes at 3 (n = 5) and 6 weeks of age (n = 3). Data are means ± s.e.m. \**P* < 0.05 and \*\*\**P* < 0.001, as determined by Welch's *t*-test. (e) MKI67-staining of the femur shown in (b). R: resting zone, P: proliferative zone, H: hypertrophic zone. Bars: 20 μm. Graphs indicate the number of MKI67-positive cells in a section of growth plate of the indicated genotypes at 3 (n = 5) and 6 weeks of age (n = 3). Data are means ± s.e.m. \**P* < 0.05 and \*\*\**P* < 0.001, as determined by Welch's *t*-test.

*Col11a2-Cre* mice. In light of previous results obtained using the same *Atg7<sup>flox/flox</sup>* mice, we conclude that deletion of *Atg7* in mesenchymal and/or prechondrogenic cells triggers activation

of some form of compensatory mechanism(s). We concluded that the impairment of autophagy from resting chondrocytes causes severe growth retardation.

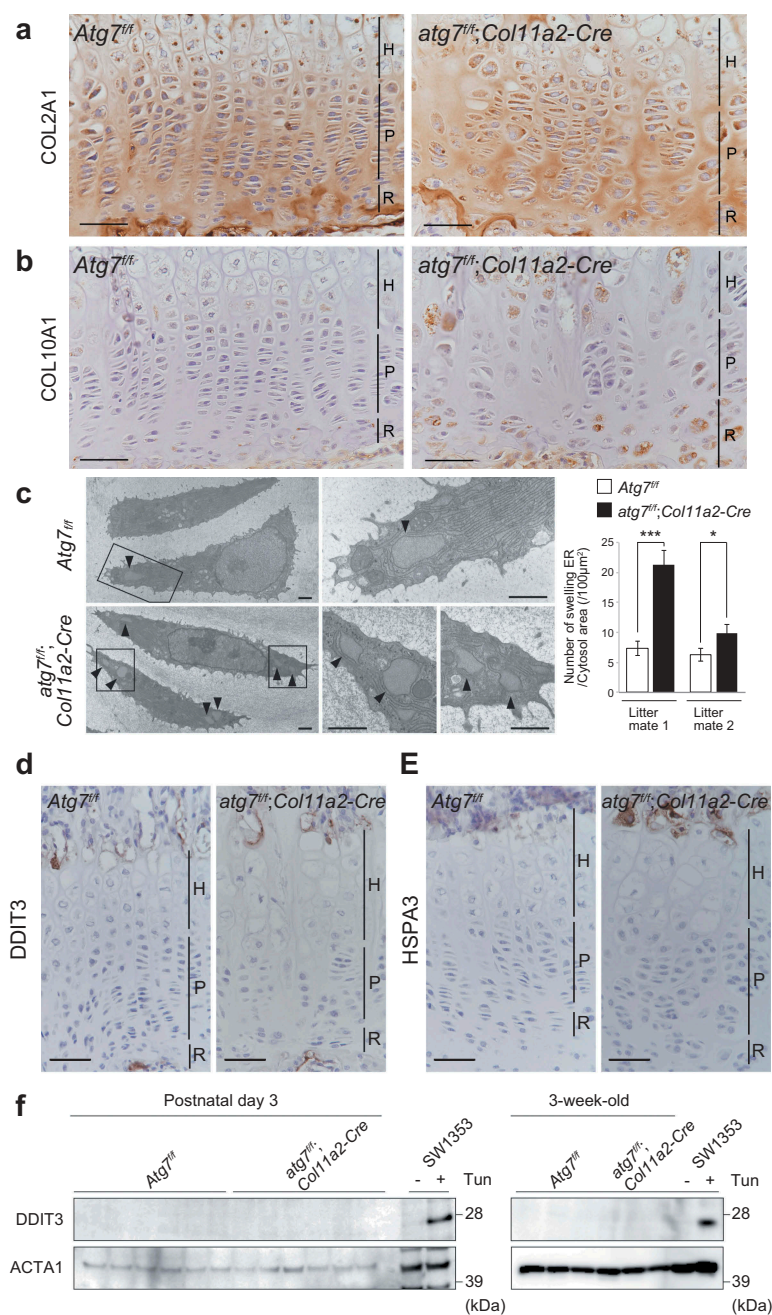


**Figure 4.** No obvious ER-stress in femur of *atg7<sup>lox/lox</sup>; Col11a2-Cre* mice. **(a and b)** Immunohistochemical staining with anti-COL2A1 (a) and anti-COL10A1 (b) antibodies of the indicated genotypes at 3 weeks of age. R: resting zone, P: proliferative zone, H: hypertrophic zone. Bars: 50 μm. **(c)** Electron microscopic analysis of proliferative chondrocytes of the indicated genotypes at 6 weeks of age. Arrowheads indicate portions of enlarged rough ER. Bars: 1 μm. Graphs indicate number of swelling ER per 100 μm<sup>2</sup> cytosolic area (n = 10) of 2 littermates. Data are means ± s.e.m. \**P* < 0.05 and \*\*\**P* < 0.001 as determined by Welch's *t*-test. **(d and e)** Immunohistochemical staining with anti-DDIT3 (d) and anti-HSPA3 (e) antibodies of growth plates from mice of the indicated genotypes at 3 weeks of age. R: resting zone, P: proliferative zone, H: hypertrophic zone. Bars: 50 μm. **(f)** Immunoblot analysis. Lysates prepared from cartilage of mice of the indicated genotype at postnatal day 3 and 3 weeks of age were subjected to immunoblotting with anti-DDIT3 and anti-ACTA1 antibodies. Lysate prepared from tunicamycin (Tun)-treated SW1353, a chondrosarcoma cell line, was used as a positive control. Data are representative of 3 separate experiments.

Why is suppression of autophagy accompanied by increased apoptosis? Using *Col2a1-Cre* mice, Kang *et al.* reported reduced height of the proliferative and hypertrophic zones in chondrocyte-specific *atg7*-knockout mice, as well as chondrocytic apoptosis throughout the zones, which is dependent on the EIF2AK3/PERK-ATF4-DDIT3/CHOP axis of the ER stress response [21]. We also observed a significantly elevated number of apoptotic cells in the proliferative zone of the growth plate in *atg7<sup>lox/lox</sup>; Col11a2-Cre* mice (Figure 3(d)). However, we observed no reduction in the

thickness of the growth plate (Figure 3(b)), probably due to compensatory swelling of both proliferating and hypertrophic chondrocytes. Unexpectedly, notwithstanding mild accumulation of COL2A1 and COL10A1 (Figure 4(a–b)) at a time when cell death of mutant chondrocytes was notable (Figure 3(d)), both our histological and biochemical analyses revealed that growth plate chondrocytes in *atg7<sup>lox/lox</sup>; Col11a2-Cre* mice did not suffer from any ER stress (Figure 4(d–f)). Therefore, ER-stress seems not



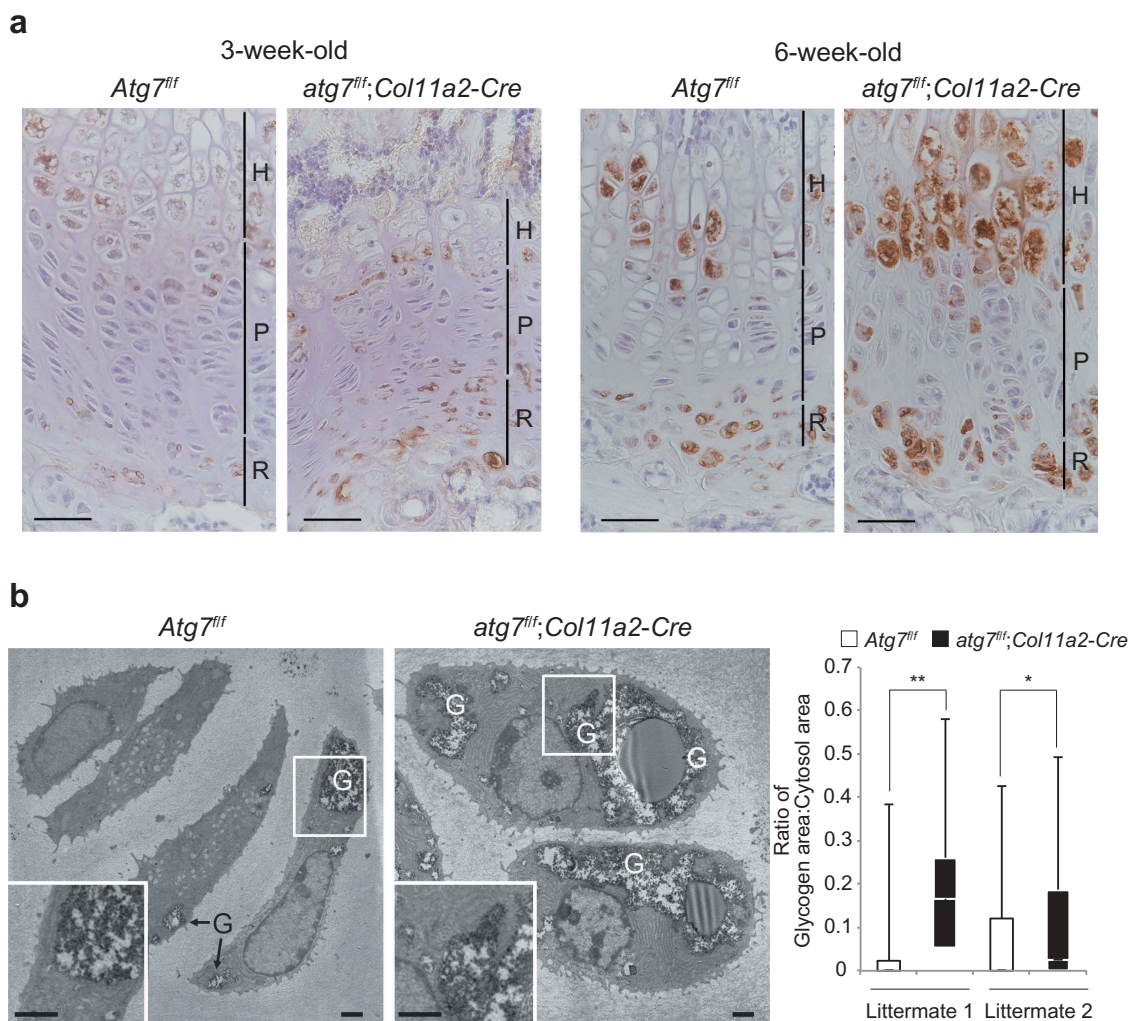


**Figure 5.** Accumulation of glycogen in chondrocytes of femur of *atg7<sup>flx/flx</sup>; Col11a2-Cre* mice. **(a)** Immunohistochemical staining with anti-glycogen antibody of femurs from mice of the indicated genotypes at 3 weeks (left panels) and 6 weeks (right panels) of age. R: resting zone, P: proliferative zone, H: hypertrophic zone. Bars: 50  $\mu$ m. **(b)** Electron microscopic analysis of resting and early proliferating chondrocytes from mice of the indicated genotypes at 6 weeks of age. Boxed regions are enlarged and shown in insets. G: glycogen area. Bars: 1  $\mu$ m. Graphs indicate the ratio of glycogen area per cytosolic area in two littermates, which are expressed as box-and-whisker plots. \* $P < 0.05$  and \*\* $P < 0.001$  as determined by Mann-Whitney  $U$  test.

to be a primary cause of cell death in chondrocytes of *atg7<sup>flx/flx</sup>; Col11a2-Cre* mice, although we cannot exclude the possibility that the chondrocytes in aged mutant mice harboring substantial accumulation of COLLAGENS (Figure S2) could suffer from ER-stress.

In all chondrocyte-specific *atg5* or *atg7*-knockout mice models, SQSTM1 is up-regulated throughout the growth plate [19–22]. SQSTM1 binds to KEAP1 (Kelch-like ECH-associated protein 1), an adaptor protein of the CUL3 (cullin 3)-based ubiquitin ligase for NFE2L2, and inhibits its E3 activity [31,32]. Thus, loss of autophagy is thought to be usually accompanied by persistent activation of NFE2L2 due to prominent accumulation of SQSTM1 [31,37]. Considering that overproduction of NFE2L2 inhibits chondrocytic differentiation [33], it is plausible that SQSTM1-mediated NFE2L2-activation may have a negative effect on chondrogenesis. However, loss of *Sqstm1* did not rescue the defective chondrogenesis observed in *atg7<sup>flx/flx</sup>; Col11a2-Cre* mice (Figure S3). Therefore, although persistent activation of NFE2L2 may inhibit the transition of mesenchymal cells to proliferating chondrocytes, it does not affect chondrogenesis from the round chondrocyte stage onward.

In chondrocytes of *atg7<sup>flx/flx</sup>; Col11a2-Cre* mice, we observed a marked accumulation of glycogen (Figure 5). Because the growth plate is an avascular structure [17,18], glycogen stored in proliferative chondrocytes in the mid-zone of the growth plate is primarily utilized as a short-term energy reserve to support cellular metabolism and biosynthesis [34,35]. This raises the possibility that glycogen accumulation in *Atg7*-deficient chondrocytes reflects a failure to supply glucose, which is essential for their survival and growth. In fact, we observed not only specific cell death of autophagy-deficient proliferative chondrocytes, but also a reduced ability to proliferate (Figure 3(d–e)). Importantly, glycogen granules are selectively enwrapped by autophagosomes for catabolism into glucose, a type of autophagy termed glycophagy [1,36]. In mechanistic terms, STBD1 (starch-binding domain-containing protein 1), which is expressed at high levels in glycogen-storage tissues, can bind glycogen through a C-terminal CBM20 glycan-binding domain, and also binds the autophagosome-localized protein GABARAP1 through its LC3-interacting region, leading to glycophagy [38,39]. A recent genetic study in mice revealed that STBD1 plays an important role in glycogen



transport to lysosomes in the liver, but not in skeletal or cardiac muscle [40]. Further analysis is needed to clarify whether STBD1-mediated glycopagy occurs chondrocytes, and if so, whether it is involved in chondrogenesis.

## Materials and methods

### Cells

ATDC5 cell lines were obtained from the RIKEN BioResource Center (RCB0565). SW1353 cell lines were obtained from ATCC (HTB-94). Cells were confirmed to be negative for mycoplasma contamination prior to use. To generate *atg7*-knockout ATDC5 cells, *Atg7* guide RNA designed using the CRISPR Design tool (<http://crispr.mit.edu/>) was subcloned into pX330-U6-Chimeric\_BB-CBh-hSpCas9 (Addgene, 42230; deposited by Feng Zhang's lab), a human codon-optimized SpCas9 and chimeric guide RNA expression plasmid. ATDC5 cells were co-transfected with vectors pX330 and pEGFP-C1 (Clontech Laboratories, 6084-1), and cultured for 2 d. Thereafter, GFP-positive cells were sorted and expanded. Loss of *Atg7* was confirmed by heteroduplex mobility assay followed by immunoblot analysis with anti-ATG7 antibody. ATDC5 cells were cultured in a DMEM/Ham's F12 medium (FUJIFILM Wako Pure Chemical Corporation, 042-30795) containing 5% fetal bovine serum, 10 µg/ml human TF (transferrin)(FUJIFILM Wako Pure Chemical Corporation, 205-18121), 30 nM sodium selenite (FUJIFILM Wako Pure Chemical Corporation, 196-10841), 2 mM L-glutamine (ThermoFisher Scientific, 25030081), 100 units/ml penicillin and 100 µg/ml streptomycin (ThermoFisher Scientific, 15140122) at 37°C in a humidified atmosphere of 5% CO<sub>2</sub> in air. To induce chondrocytic differentiation, human INSULIN (10 mg/ml) (FUJIFILM Wako Pure Chemical Corporation, 093-06471) was added to the medium, and the cells were cultured for 3 weeks [27]. Medium was replaced every 2 or 3 d [27]. SW1353 cells were cultured in Leibovitz's L-15 medium (ThermoFisher Scientific, 11415064) containing 10% non-inactivated fetal bovine serum, 2 mM L-glutamine (ThermoFisher Scientific, 25030081), 100 units/ml penicillin and 100 µg/ml streptomycin (ThermoFisher Scientific, 15140122) at 37°C in a humidified atmosphere. To induce ER-stress response, Tunicamycin (5 µg/ml) (Sigma-Aldrich, T7765) was added to the medium, and the cells were cultured for 12 h.

### Mice

*Atg7<sup>lox/flox</sup>* [30], and *Sqstm1<sup>lox/flox</sup>* [29] mice in the C57BL/6 genetic background were used in this study. *Atg7<sup>lox/flox</sup>*, and *Atg7<sup>lox/flox</sup>; Sqstm1<sup>lox/flox</sup>* mice were bred with *Col11a2-Cre* mice [26] to generate *atg7<sup>lox/flox</sup>; Col11a2-Cre* and *atg7<sup>lox/flox</sup>; sqstm1<sup>lox/flox</sup>; Col11a2-Cre* mice, respectively. Mice were housed in specific pathogen-free facilities, and the Ethics Review Committee for Animal Experimentation of Niigata University approved the experimental protocol.

### Immunoblot analysis

Cartilage was homogenized in 0.25 M sucrose, 10 mM 2-[4-(2-hydroxyethyl)-1-piperazinyl]ethanesulfonic acid (pH 7.4), and 1 mM dithiothreitol (Sigma-Aldrich, D9779). Samples were subjected to SDS-PAGE, and then transferred to a polyvinylidene difluoride membrane (Merck, IPVH00010). Antibodies against ATG7 (FUJIFILM Wako Pure Chemical Corporation, 013-22831; 1:1000), LC3B (Cell Signaling Technology, 2775; 1:1000), SQSTM1/p62 (Medical & Biological Laboratories Co., PM066; 1:1000), COL2A1/COLLAGEN II (Abcam, ab34712; 1:1000), DDIT3/CHOP (Cell Signaling Technology, 2895; 1:1000), and ACTA1/ACTIN (Merck, MAB1501R; 1:1000) were purchased from the indicated suppliers. Blots were incubated with horseradish peroxidase-conjugated goat anti-mouse IgG (H + L) (Jackson ImmunoResearch Laboratories, Inc., 115-035-166), goat anti-rabbit IgG (H + L) (Jackson ImmunoResearch Laboratories, Inc., 111-035-144) or goat anti-guinea pig IgG(H + L) antibody (Jackson ImmunoResearch Laboratories, Inc., 106-035-003), and then visualized by chemiluminescence. Density of the bands was quantified by Multi Gauge V3.2 software (FUJIFILM Corporation, Tokyo, Japan).

### Soft X-ray radiography and skeletal staining

For soft X-ray analysis, mice were examined on a SOFRON SRO-M40 (Sofron Co. Ltd, Tokyo, Japan). Exposures were at 30 kV and 4 mA and lasted for 20 s. Next, the samples were fixed for 2 d with 95% ethanol at room temperature and stained with Alcian blue solution containing 0.015% Alcian blue 8GX (Sigma-Aldrich, 05500), 20% acetic acid, and 80% ethanol. After 24 h, skeleton samples were rinsed with 95% ethanol and 2% KOH and counterstained overnight with 0.005% alizarin red S (NACALAI TESQUE, INC., 01303-52) in 2% KOH for 5 h at room temperature. After rinsing with water, samples were cleared with 2% KOH; transferred sequentially into 20%, 40%, and 60% glycerol; and stored in 80% glycerol (FUJIFILM Wako Pure Chemical Corporation, 075-00611).

### Histological experiments

Mice were perfused with 4% paraformaldehyde, and excised femurs were decalcified with 10% EDTA, pH7.4 for 2 weeks at 4°C. Paraffin sections with 4 µm thickness were processed for immunohistochemistry. For antigen retrieval, sections were treated with 0.15% trypsin (Sigma-Aldrich, T7409) in 10 mM Tris-HCl (pH 7.6) for 15 min at 37°C. After blocking with 5% skimmed milk in PBS (145 mM NaCl, 2 mM NaH<sub>2</sub>PO<sub>4</sub>, 8 mM Na<sub>2</sub>HPO<sub>4</sub>) and 0.05% Triton X-100 (NACALAI TESQUE, INC., 35501-15), sections were incubated for 1 d at 4°C with primary antibodies against ATG7 (FUJIFILM Wako Pure Chemical Corporation, 013-22831; 1:200), SQSTM1/p62 (Progen Biotechnik GmbH, GP62-C; 1:200), MAP1LC3A (Abcam, ab52768; 1:500), MKI67/Ki67 (Dako, M7249; 1:100), COL2A1/COLLAGEN II (Abcam, ab34712; 1:400), COL10A1/COLLAGEN X (LSL Ltd, LSL-LB-0092; 1:200), DDIT3/CHOP (Cell Signaling Technology, 9204S; 1:100),

HSPA3/BIP (Cell Signaling Technology, 3177; 1:200) and glycogen [41] (1:100). After incubation with primary antibodies, sections were incubated with the Envision+HRP system (Dako, K4061) or biotinylated secondary antibodies for 1 h, followed by exposure to streptavidin-peroxidase complex (Vector Laboratories, Inc., PK-6100) for 1 h. For visualization of reaction products, sections were treated with 0.02% 3,3'-diaminobenzidine (Dojindo Laboratories, D006) and counterstained with hematoxylin (Dako, S2020). For immunofluorescence staining, Alexa Fluor-488-conjugated donkey anti-rabbit IgG (Thermo Fisher scientific, A11008) and Alexa Fluor-568-conjugated goat anti-guinea pig IgG (Thermo Fisher scientific, A11057) were used as secondary antibodies. Sections were counterstained with DAPI (Vector Laboratories, Inc., H-1200) or PI (Vector Laboratories, Inc., H-1300) and observed with a fluorescence microscope (BX51) (Olympus, Tokyo, Japan) or a laser scanning confocal microscope (Olympus, FV300). After image acquisition, contrast and brightness were adjusted using Photoshop CS4 (Adobe Systems, Inc., San Jose, CA, USA). The method for the TUNEL assay was described previously [42]. To count TUNEL-positive cells in the growth plate, a total of 6 and 2 areas for each individual were calculated in 3- (n = 5) and 6-week-old mice (n = 3), respectively. To count MKI67-positive cells in the growth plate, a total of 3 and 2 areas for each individual were calculated in 3- (n = 5) and 6-week-old mice (n = 3), respectively.

### Electron microscopy

6-week-old mice were anesthetized with Isoflurane (FUJIFILM Wako Pure Chemical Corporation, 099-06571), followed by pentobarbital (25 mg/kg ip). They were then perfused via the heart first with ~30 ml of Ringer's solution (Otsuka Pharmaceutical Factory, Inc., 873319) containing 10 U/ml heparin (NACALAI TESQUE, INC., 17513-54), and then with 50 ml of 0.1 M phosphate buffer (pH 7.4) containing 2% paraformaldehyde (Merck, 30525-89-4) and 2% glutaraldehyde (TAAB Laboratories Equipment Ltd, G011/1). Femurs were excised and further fixed by immersing in the same fixative for 2 d, and then demineralized by slowly shaking in a solution of 10% EDTA-2Na (pH 7.3) at room temperature for 17 d. The growth plate of the distal part was cut so that the directions can be recognized. Samples were then postfixed for 180 min at 4°C with 1% OsO<sub>4</sub> (Merck, 124505)-1.5% tetrapotassium ferrocyanide (FUJIFILM Wako Pure Chemical Corporation, 152560) in H<sub>2</sub>O. Conventional dehydration and embedding procedures were performed as reported previously [43]. Ultra-thin sections of 60-nm thickness were stained with uranyl acetate (FUJIFILM Wako Pure Chemical Corporation, 219-00692) and lead citrate (TAAB Laboratories Equipment Ltd, L018), and observed under an electron microscope, JEM1400EX (JEOL, Tokyo, Japan).

For counting dilated ER, profiles of proliferating chondrocytes were taken at a magnification of x 6000, while for the estimation of glycogen contents, resting and early proliferating cells that resided within a zone approximately 30 μm from the bone-cartilage boundary were taken at x 8000. Both cytoplasmic and glycogen areas were measured using ImageJ (National Institutes of Health, Bethesda, MD, USA).

### Statistical analysis

Statistical analysis was performed using the unpaired *t*-test (Welch test) or Mann-Whitney U test. A *P* value less than 0.05 was considered to indicate statistical significance.

### Acknowledgments

We thank M. Takasaki, A. Yabashi and M. Abe (Fukushima Medical University) for their technical help in electron microscopy. M.K. is supported by Grants-in-Aid for Scientific Research on Innovative Areas (JP25111006 to M.K.), the Japan Society for the Promotion of Science (an A3 foresight program, to M.K., 15H06600), and the Takeda Science Foundation (to M.K.).

### Disclosure statement


No potential conflict of interest was reported by the authors.

### Funding

This work was supported by the Japan Society for the Promotion of Science [15H06600]; Japan Society for the Promotion of Science [JP25111006].

### ORCID

Shunichi Shibata  <http://orcid.org/0000-0003-3412-7002>

Masaaki Komatsu  <http://orcid.org/0000-0001-7672-7722>

### References

- [1] Kaur J, Debnath J. Autophagy at the crossroads of catabolism and anabolism. *Nat Rev Mol Cell Biol.* 2015;16:461–472.
- [2] Kroemer G, Marino G, Levine B. Autophagy and the integrated stress response. *Mol Cell.* 2010;40:280–293.
- [3] Mizushima N, Komatsu M. Autophagy: renovation of cells and tissues. *Cell.* 2011;147:728–741.
- [4] Kuma A, Hatano M, Matsui M, et al. The role of autophagy during the early neonatal starvation period. *Nature.* 2004;432:1032–1036.
- [5] Karsli-Uzunbas G, Guo JY, Price S, et al. Autophagy is required for glucose homeostasis and lung tumor maintenance. *Cancer Discov.* 2014;4:914–927.
- [6] Singh R, Kaushik S, Wang Y, et al. Autophagy regulates lipid metabolism. *Nature.* 2009;458:1131–1135.
- [7] Rambold AS, Cohen S, Lippincott-Schwartz J. Fatty acid trafficking in starved cells: regulation by lipid droplet lipolysis, autophagy, and mitochondrial fusion dynamics. *Dev Cell.* 2015;32:678–692.
- [8] Devos P, Hers HG. Random, presumably hydrolytic, and lysosomal glycogenolysis in the livers of rats treated with phlorizin and of newborn rats. *Biochem J.* 1980;192:177–181.
- [9] Schiaffino S, Mammucari C, Sandri M. The role of autophagy in neonatal tissues: just a response to amino acid starvation? *Autophagy.* 2008;4:727–730.
- [10] Mizushima N, Levine B. Autophagy in mammalian development and differentiation. *Nat Cell Biol.* 2010;12:823–830.
- [11] Zhang Y, Goldman S, Baerga R, et al. Adipose-specific deletion of autophagy-related gene 7 (*atg7*) in mice reveals a role in adipogenesis. *Proc Natl Acad Sci U S A.* 2009;106:19860–19865.
- [12] Mortensen M, Ferguson DJ, Edelmann M, et al. Loss of autophagy in erythroid cells leads to defective removal of mitochondria and severe anemia in vivo. *Proc Natl Acad Sci U S A.* 2010;107:832–837.

- [13] Tsukamoto S, Kuma A, Murakami M, et al. Autophagy is essential for preimplantation development of mouse embryos. *Science*. 2008;321:117–120.
- [14] Toshima T, Shirabe K, Fukuhara T, et al. Suppression of autophagy during liver regeneration impairs energy charge and hepatocyte senescence in mice. *Hepatology*. 2014;60:290–300.
- [15] Altshuler-Keylin S, Shinoda K, Hasegawa Y, et al. Beige adipocyte maintenance is regulated by autophagy-induced mitochondrial clearance. *Cell Metab*. 2016;24:402–419.
- [16] Kronenberg HM. Developmental regulation of the growth plate. *Nature*. 2003;423:332–336.
- [17] Srinivas V, Bohensky J, Zahm AM, et al. Autophagy in mineralizing tissues: microenvironmental perspectives. *Cell Cycle*. 2009;8:391–393.
- [18] Shapiro IM, Layfield R, Lotz M, et al. Boning up on autophagy: the role of autophagy in skeletal biology. *Autophagy*. 2014;10:7–19.
- [19] Cinque L, Forrester A, Bartolomeo R, et al. FGF signalling regulates bone growth through autophagy. *Nature*. 2015;528:272–275.
- [20] Vuppapapati KK, Boudierlique T, Newton PT, et al. Targeted deletion of autophagy genes Atg5 or Atg7 in the chondrocytes promotes caspase-dependent cell death and leads to mild growth retardation. *J Bone Miner Res*. 2015;30:2249–2261.
- [21] Kang X, Yang W, Feng D, et al. Cartilage-specific autophagy deficiency promotes ER stress and impairs chondrogenesis in PERK-ATF4-CHOP-dependent manner. *J Bone Miner Res*. 2017;32:2128–2141.
- [22] Boudierlique T, Vuppapapati KK, Newton PT, et al. Targeted deletion of Atg5 in chondrocytes promotes age-related osteoarthritis. *Ann Rheum Dis*. 2016;75:627–631.
- [23] Logan M, Martin JF, Nagy A, et al. Expression of Cre Recombinase in the developing mouse limb bud driven by a Prxl enhancer. *Genesis*. 2002;33:77–80.
- [24] Ovchinnikov DA, Deng JM, Ogunrinu G, et al. Col2a1-directed expression of Cre recombinase in differentiating chondrocytes in transgenic mice. *Genesis*. 2000;26:145–146.
- [25] Nakamura E, Nguyen MT, Mackem S. Kinetics of tamoxifen-regulated Cre activity in mice using a cartilage-specific CreER(T) to assay temporal activity windows along the proximodistal limb skeleton. *Dev Dyn*. 2006;235:2603–2612.
- [26] Iwai T, Murai J, Yoshikawa H, et al. Smad7 inhibits chondrocyte differentiation at multiple steps during endochondral bone formation and down-regulates p38 MAPK pathways. *J Biol Chem*. 2008;283:27154–27164.
- [27] Shukunami C, Ishizeki K, Atsumi T, et al. Cellular hypertrophy and calcification of embryonal carcinoma-derived chondrogenic cell line ATDC5 in vitro. *J Bone Miner Res*. 1997;12:1174–1188.
- [28] Kabeya Y, Mizushima N, Ueno T, et al. LC3, a mammalian homologue of yeast Apg8p, is localized in autophagosome membranes after processing. *Embo J*. 2000;19:5720–5728.
- [29] Komatsu M, Waguri S, Koike M, et al. Homeostatic levels of p62 control cytoplasmic inclusion body formation in autophagy-deficient mice. *Cell*. 2007;131:1149–1163.
- [30] Komatsu M, Waguri S, Ueno T, et al. Impairment of starvation-induced and constitutive autophagy in Atg7-deficient mice. *J Cell Biol*. 2005;169:425–434.
- [31] Komatsu M, Kurokawa H, Waguri S, et al. The selective autophagy substrate p62 activates the stress responsive transcription factor Nrf2 through inactivation of Keap1. *Nat Cell Biol*. 2010;12:213–223.
- [32] Lau A, Wang XJ, Zhao F, et al. A noncanonical mechanism of Nrf2 activation by autophagy deficiency: direct interaction between Keap1 and p62. *Mol Cell Biol*. 2010;30:3275–3285.
- [33] Hinoi E, Takarada T, Fujimori S, et al. Nuclear factor E2 p45-related factor 2 negatively regulates chondrogenesis. *Bone*. 2007;40:337–344.
- [34] Otte P. Basic cell metabolism of articular cartilage. Manometric studies. *Z Rheumatol*. 1991;50:304–312.
- [35] Pritchard JJ. A cytological and histochemical study of bone and cartilage formation in the rat. *J Anat*. 1952;86:259–277.
- [36] Ueno T, Komatsu M. Autophagy in the liver: functions in health and disease. *Nat Rev Gastroenterol Hepatol*. 2017;14:170–184.
- [37] Ichimura Y, Waguri S, Sou YS, et al. Phosphorylation of p62 activates the Keap1-Nrf2 pathway during selective autophagy. *Mol Cell*. 2013;51:618–631.
- [38] Jiang S, Heller B, Tagliabracci VS, et al. Starch binding domain-containing protein 1/genethonin 1 is a novel participant in glycogen metabolism. *J Biol Chem*. 2010;285:34960–34971.
- [39] Jiang S, Wells CD, Roach PJ. Starch-binding domain-containing protein 1 (Stbd1) and glycogen metabolism: identification of the Atg8 family interacting motif (AIM) in Stbd1 required for interaction with GABARAPL1. *Biochem Biophys Res Commun*. 2011;413:420–425.
- [40] Sun T, Yi H, Yang C, et al. Starch binding domain-containing protein 1 plays a dominant role in glycogen transport to lysosomes in liver. *J Biol Chem*. 2016;291:16479–16484.
- [41] Baba O. Production of monoclonal antibody that recognizes glycogen and its application for immunohistochemistry. *Kokubyo Gakkai Zasshi*. 1993;60:264–287.
- [42] Ida-Yonemochi H, Nakatomi M, Harada H, et al. Glucose uptake mediated by glucose transporter 1 is essential for early tooth morphogenesis and size determination of murine molars. *Dev Biol*. 2012;363:52–61.
- [43] Waguri S, Komatsu M. Biochemical and morphological detection of inclusion bodies in autophagy-deficient mice. *Methods Enzymol*. 2009;453:181–196.